

# UC San Diego

## UC San Diego Previously Published Works

### Title

Numerical Modeling of a Soil-Borehole Thermal Energy Storage System

### Permalink

<https://escholarship.org/uc/item/4n65g24p>

### Journal

Vadose Zone Journal, 15(1)

### ISSN

1539-1663

### Authors

Catolico, Nora  
Ge, Shemin  
McCartney, John S

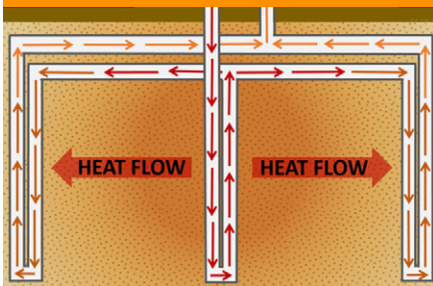
### Publication Date

2016

### DOI

10.2136/vzj2015.05.0078

Peer reviewed

**Core Ideas:**

- Borehole thermal energy storage is studied with a 3D transient fluid flow and heat transfer model.
- BTES heat extraction efficiency increases with decreasing soil thermal conductivity.
- BTES efficiency decreases with convective heat losses associated with high soil permeability.

N. Catolico and S. Ge, Dep. of Geological Sciences, Univ. of Colorado, UCB 399, Boulder, CO 80309-0399; J.S. McCartney, Dep. of Structural Engineering, Univ. of California–San Diego, 9500 Gilman Drive, Mail Code 0085, La Jolla, CA 92093-0085. \*Corresponding author (Ges@colorado.edu).

Vadose Zone J.  
doi:10.2136/vzj2015.05.0078  
Received 22 May 2015.  
Accepted 9 Oct. 2015.  
Open access article.  
Supplemental material online.

Vol. 15, Iss. 1, 2016  
© Soil Science Society of America. This is an open access article distributed under the CC BY-NC-ND license (<http://creativecommons.org/licenses/by-nc-nd/4.0/>).

# Numerical Modeling of a Soil-Borehole Thermal Energy Storage System

Nora Catolico, Shemin Ge,\* and John S. McCartney

Borehole thermal energy storage (BTES) in soils combined with solar thermal energy harvesting is a renewable energy system for the heating of buildings. The first community-scale BTES system in North America was installed in 2007 at the Drake Landing Solar Community (DLSC) in Okotoks, AB, Canada, and has since supplied >90% of the thermal energy for heating 52 homes. A challenge facing BTES system technology is the relatively low efficiency of heat extraction. To better understand the fluid flow and heat transport processes in soils and to improve BTES efficiency of heat extraction for future applications, a three-dimensional transient coupled fluid flow and heat transfer model was established using TOUGH2. Measured time-dependent injection temperatures and fluid circulation rates at DLSC were used as model inputs. The simulations were calibrated using measured soil temperature time series. The simulated and measured temperatures agreed well with a subsurface having an intrinsic permeability of  $1.5 \times 10^{-14} \text{ m}^2$ , thermal conductivity of  $2.0 \text{ W m}^{-1} \text{ }^\circ\text{C}^{-1}$ , and a volumetric heat capacity of  $2.3 \text{ MJ m}^{-3} \text{ }^\circ\text{C}^{-1}$ . The calibrated model served as the basis for a sensitivity analysis of soil thermal and hydrological parameters on BTES system heat extraction efficiency. Sensitivity analysis results suggest that: (i) BTES heat extraction efficiency increases with decreasing soil thermal conductivity; (ii) BTES efficiency decreases with background groundwater flow; (iii) BTES heat extraction efficiency decreases with convective heat losses associated with high soil permeability values; and (iv) unsaturated soils show higher overall heat extraction efficiency due to convection onset at higher intrinsic permeability values.

Abbreviations: BTES, borehole thermal energy storage; DLSC, Drake Landing Solar Community.

**Growing concerns** about greenhouse gas emissions and fossil fuel consumption have motivated the increased development of renewable energy systems including solar thermal energy harvesting technologies for the heating and cooling of buildings. In recent decades, borehole thermal energy storage (BTES) systems with heat derived from solar technology are rapidly gaining attention and use worldwide (Claesson and Hellstrom 1981; Dalenbäck and Jilar, 1985; Nordell and Hellström, 2000; Sanner and Knoblich, 1999; Sanner et al., 2003; Morofsky, 2007; Sibbitt et al., 2007, 2011, 2012; Wang et al., 2010; Dehkordi and Schincariol, 2014a; Acuna and Palm, 2013; Başer and McCartney, 2015). In BTES systems, a series of U-tube pipes placed in closely spaced (1.5–2.5 m) vertical boreholes are connected to form a closed-loop heat exchanger (Fig. 1). Heat exchange is achieved by circulation of a heat carrier fluid through the closed-loop U-tube pipes. Many BTES systems store heat collected from solar thermal panels in the summer months until it can be extracted for use during the winter months. These thermal energy storage systems present a potentially economical and environmentally sustainable alternative to traditional heating systems because they permit the storage of renewable energy in a space-efficient manner underground.

A major challenge facing BTES systems is their relatively low heat extraction efficiency. Annual efficiency is a measure of a thermal energy storage system's performance, defined as

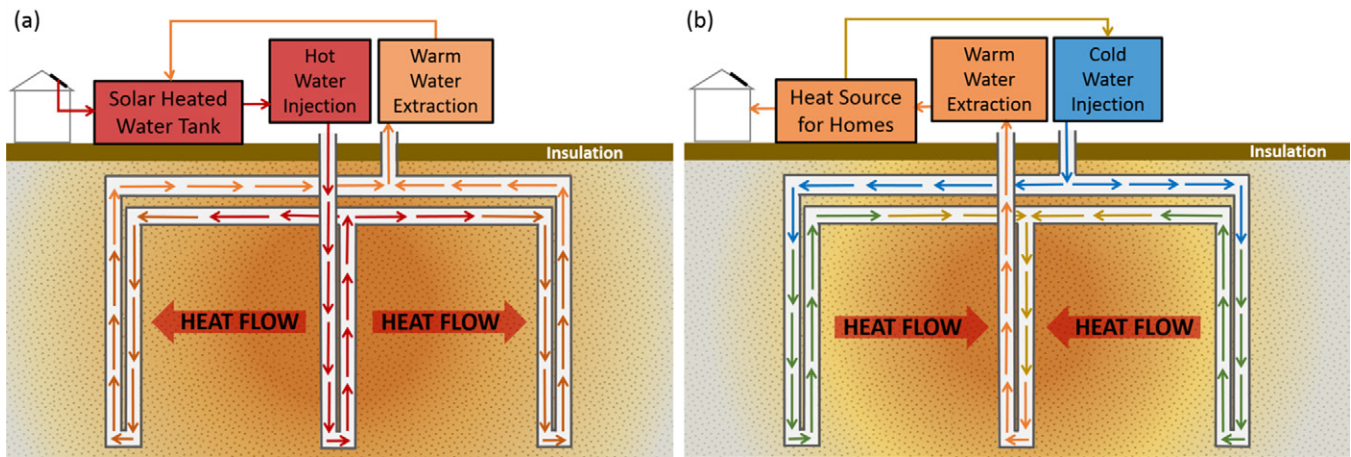


Fig. 1. Simplified schematic of a borehole thermal energy storage system during (a) summer heat storage of solar energy (charging) and (b) winter heat extraction (discharging).

the ratio of the total energy recovered from the subsurface storage to the total energy injected during a yearly cycle (Dincer and Rosen, 2007). Efficiencies for the first 6 yr of operation of the BTES system at the DLSC range from 6 to 54% (Sibbitt et al., 2011). Nonetheless, the BTES system at DLSC is still able to supply >90% of the thermal energy for heating 52 homes (Sibbitt et al., 2012).

Few studies have investigated the impact of hydrologic parameters on the efficiency of BTES. Common guidelines require a subsurface that is drillable, of high heat capacity, and with low hydraulic conductivity (Schmidt et al., 2003; Pavlov and Olesen, 2012). Several factors may affect BTES system performance, including the volume and geometry of storage space, the number and dimensions of boreholes, the injection–extraction scheme, and the soil and rock mechanical, hydrological, and thermal properties (Ohga and Mikoda, 2001; Dehkordi and Schincariol, 2014b; Başer and McCartney 2015). The influences of these factors are poorly understood, and no specific parameter guidelines have been suggested for enhancing the efficiency of BTES systems. Advancements in the understanding of the specific effects of these parameters are needed because improved efficiency would greatly increase the economic viability of BTES technology.

In the past few decades, numerical modeling has become the standard in the analysis of geothermal energy systems (Breger et al., 1996; O’Sullivan et al., 2001; Diersch et al., 2011); however, models that study the parameters affecting the performance of BTES systems are lacking. Existing models of thermal energy storage systems are limited to aquifer thermal energy storage systems (Molson et al., 1992; Tenma et al., 2003; Lee, 2008, 2010; Lee and Sang, 2008; Sommer et al., 2013). These studies focused on the configuration of borehole design and operational parameters in such systems. Recent studies have been primarily concerned with engineering layout (Lanini et al., 2014; Başer and McCartney, 2015) and modeling methodology (Lazzarotto, 2014). Dehkordi and Schincariol (2014b) examined the sensitivity of a single borehole heat exchanger

system to thermal–hydrogeological properties; however, they did not consider the role of such properties in a system that incorporates thermal energy additions to the subsurface. Existing models have not explored the role of soil thermal and hydrological properties such as thermal conductivity, permeability, and degree of saturation on BTES system performance, nor have they looked at the effect of groundwater flow on a multi-borehole system. There exists a critical need for numerical modeling to be applied to these BTES scenarios to better understand heat transport in BTES systems and provide guidance for site selection and system design.

The objective of this study was to examine how soil hydrological and thermal parameters affect the BTES system efficiency. Little is known about the role of site geology in BTES systems despite the subsurface acting as its primary means of thermal storage. Several questions were raised: How do thermal properties of the soil affect BTES system efficiency? How will background groundwater flow affect the BTES system’s ability to store thermal energy? How will the soil permeability affect its ability to store and transfer heat? Will heat transfer processes differ with the degree of saturation in a way that will significantly affect BTES efficiency? To address these questions, a three-dimensional transient coupled fluid and heat transfer model was developed to simulate heat transport in soils for an existing BTES system at DLSC. The model was calibrated using field data from the existing BTES system. The calibrated model was then used as a basis to analyze the BTES system’s sensitivity to soil thermal conductivity, hydraulic gradient, saturated soil permeability, and unsaturated soil permeability.

## Drake Landing Borehole Thermal Energy Storage System

Drake Landing Solar Community (DLSC), located in Okotoks, AB, Canada, consists of 52 houses, an 800-panel garage-mounted

array of solar collectors, short-term thermal storage tanks, and approximately 34,000 m<sup>3</sup> of subsurface BTES space (Drake Landing Solar Community, 2015). The BTES system is comprised of 24 series of six connected U-tube pipes that extend from the center to the outer boundary in a radial direction (Fig. 2). During charging, heated fluid is circulated into the boreholes at the center of the array first, then progressively through boreholes toward the boundary. In this case, the center of the array reaches the greatest temperatures. During the winter discharging months, cold water is injected into the outer boundary pipes, is heated by the thermal energy stored in the soil, and then is extracted from the center pipes. The warm water is pumped to the homes and heat is transferred to the homes through forced-air-fan coil units. The system is bounded above by an insulation layer and hydraulic barrier that prevent heat and fluid exchange with the surface (Fig. 2).

No report on soil properties is available for the DLSC; however, a geotechnical analysis was conducted in 2004 at the nearby Twin Valley Resort (G Tech Earth Sciences Corp, 2004). In this study, 15 test boreholes were drilled to study the geology of the subsurface. The holes showed a near-surface layer averaging 4.07 m thick that varied among silty, clayey, and gravely sands. In all cases, this layer overlaid glacial clay till or bedrock. The water table ranged between 2.64 and 5.90 m below the surface. Surface temperatures annually average 5°C but can range from 37°C in the summer to -35°C in the winter. The system has been operational since 12 Apr. 2007. Recorded data are available since 1 July 2007 including: (i) temperature and flow rates of injection and extraction; (ii) temperature for a lateral array of sensors near and below the ground surface between the vertical boreholes; and (iii) temperature at

varied depths representing core BTES temperatures near the center of the system.

Annual heat extraction efficiency is the parameter of interest. Heat extraction efficiency ( $E$ ) is computed as the ratio of the energy extracted from the system during discharging periods ( $J_{out}$ ) to the total energy injected into the system during charging periods ( $J_{in}$ ):

$$E = \frac{J_{out}}{J_{in}} \quad [1]$$

where

$$J_{out} = \sum_{j=1}^n (T_{c_j} - T_{o_j}) Q_j \Delta t_j c \rho B \quad [2]$$

and

$$J_{in} = \sum_{j=1}^m (T_{c_j} - T_{o_j}) Q_j \Delta t_j c \rho B \quad [3]$$

where  $T_{c_j}$  is the temperature at the center boreholes (°C),  $T_{o_j}$  is the temperature at the outer boreholes (°C),  $Q_j$  is the volumetric flow rate (m<sup>3</sup> s<sup>-1</sup>),  $\Delta t_j$  is the  $j$ th time interval (s),  $c$  is the heat capacity of water (J kg<sup>-1</sup> °C<sup>-1</sup>),  $\rho$  is the density of water (kg m<sup>-3</sup>), and  $B$  is the number of borehole series, 24 in the case of Fig. 2. The index  $j$  represents the  $j$ th time interval,  $n$  is the total discharging stress periods, and  $m$  is the total charging stress periods for the given year. All borehole series are assumed to have the same injection-extraction temperature and flow rates. Calculated efficiencies for the first 6 yr of operation at the DLSC are 4.6, 18.4, 35.9, 53.8, 35.8, and 50.9%, respectively. The stress period can be either a charging or discharging phase based on which phase dominates during that period.

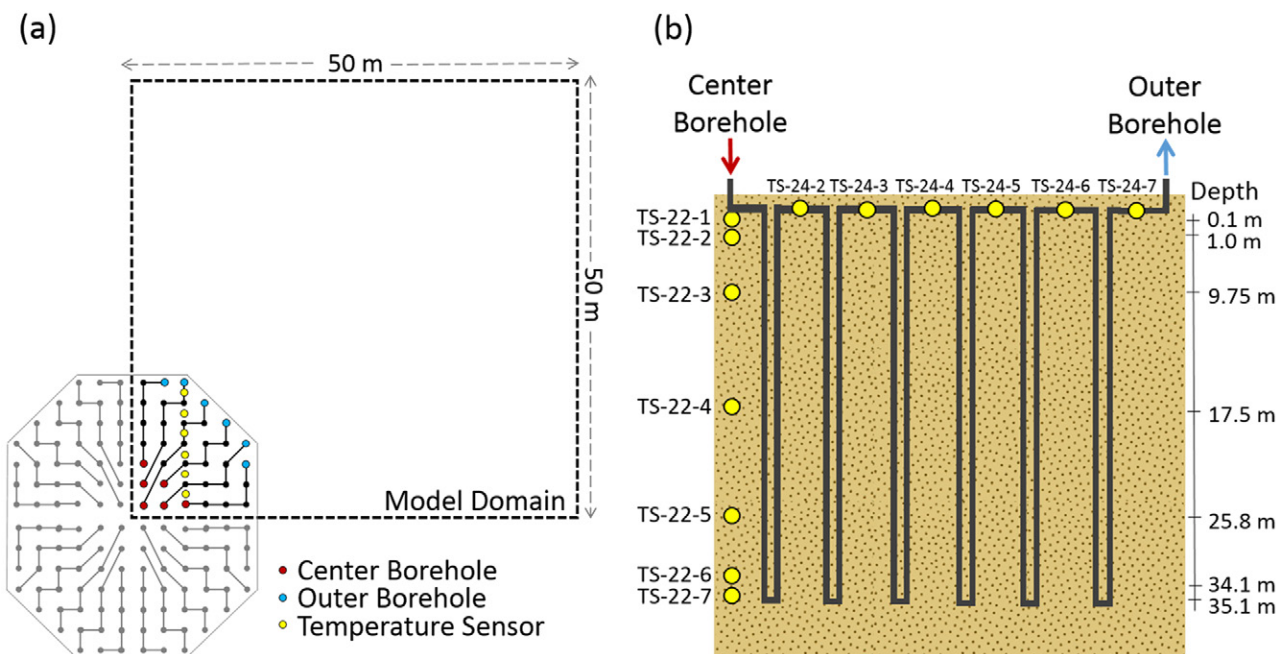


Fig. 2. (a) Plan view of the simulated borehole region showing location of the temperature sensors and piping within the model domain; and (b) cross-section showing the locations of lateral and core temperature sensors along one series of U-tube piping.



conditions were assigned to represent the in situ conditions. A calibrated temperature of 8.1°C and hydrostatic pressure were imposed at the two far-field boundaries and the bottom boundary. The far-field and bottom boundaries are sufficiently distant from the borehole area so that the boundary conditions do not affect the resulting temperatures. The top boundary was set to the annual average surface temperature of 5.1°C and a pressure of  $1.0 \times 10^5$  Pa. By symmetry, a zero temperature gradient and zero pressure gradient boundary condition were imposed on the vertical planes that cross the center of the BTES system.

An intrinsic permeability of  $1.5 \times 10^{-14}$  m<sup>2</sup> is representative for the glacial till (Fetter, 2001) present at the site. The sensitivity of BTES system performance to this value is examined below. Thermal conduction was allowed between the pipe cells and the surrounding medium. Within the pipe cells, we set the thermal conductivity to that of the carrier fluid. Between the pipe cells and the surrounding medium, the thermal conductivity is equal to that of the piping material. A thermal conductivity of 0.51 W m<sup>-1</sup> °C<sup>-1</sup> was used to represent the polyethylene U-tube piping. Between the piping and ground surface is an insulation layer with a thermal conductivity of 0.23 W m<sup>-1</sup> °C<sup>-1</sup> (Zhang et al., 2012). The low thermal conductivity of the insulating layer allows some minimal heat loss, as would be expected in the real-life scenario but is sufficient to support a constant-temperature boundary condition for the time and spatial scales considered in our model. For simplicity, this layer extends across the entire top of the model, although at the site this insulation layer only overlaps the BTES system by 5 m. In a real-life scenario, it could be conceived that once the thermal plume extended radially beyond the bounds of the insulated area, greater heat loss to the surface would occur. The relevant properties of the different materials are summarized in Table 1.

The time period of interest is from July 2007 to July 2013, for which measured temperature and flow rate data were available from the DLSC site. A transient simulation was necessary because injection temperatures and fluid circulation rates varied with time. The data showed that the flow direction changed frequently, sometimes reversing multiple times during the course of a single day (Fig. 4, light red and light blue dots), making it difficult to set up a true time-dependent flow rate for the numerical model. We approached this issue by dividing each year into representative charging and

Table 1. Material properties of the Drake Landing borehole thermal energy storage system for the three-dimensional fluid flow and heat transfer model.

Parameter	Value
Soil particle density, kg m <sup>-3</sup> †	2480
Soil permeability, m <sup>2</sup>	$1.5 \times 10^{-14}$
Soil thermal conductivity, W m <sup>-1</sup> °C <sup>-1</sup> †	2.03
Soil porosity, m <sup>3</sup> m <sup>-3</sup> †	0.50
Soil heat capacity, J kg <sup>-1</sup> °C <sup>-1</sup> †	935.80
Fluid density, kg m <sup>-3</sup>	1000
Fluid heat capacity, J kg <sup>-1</sup> °C <sup>-1</sup>	4183
U-tube thermal conductivity, W m <sup>-1</sup> °C <sup>-1</sup>	0.51
Insulation layer thermal conductivity, W m <sup>-1</sup> °C <sup>-1</sup> †	0.23
U-tube radius, m	0.055

† Properties taken from Zhang et al. (2012).

discharging stress periods, yielding between 7 and 15 stress periods per year (Fig. 4, dark red and dark blue lines), respectively, or 66 total stress periods during 6 yr. To ensure that the overall heat injection and extraction were representative and accurate for energy balance, the following energy equivalence calculation was used to obtain the average injection temperatures for each stress period:

$$T_{i\text{-avg}} = \frac{\sum_{j=1}^n T_j q_j \Delta t_j c}{\sum_{j=1}^n q_j \Delta t_j c} \quad [4]$$

where the index *i* represents the stress period, index *j* represents the *j*th time interval within the *i*th period, *T<sub>j</sub>* is the measured temperature at the injection boreholes (°C), *q<sub>j</sub>* is the measured mass flow rate (kg s<sup>-1</sup>), Δ*t<sub>j</sub>* is the *j*th time interval within the period, and *c* is the specific heat capacity of water (J kg<sup>-1</sup> °C<sup>-1</sup>). Approximated temperatures and stress periods are shown in Fig. 4. The value of *T<sub>i-avg</sub>* for the charging periods was calculated using the temperature data from the center boreholes when fluid was injected in the center boreholes and extracted at the outer boreholes. The value of *T<sub>i-avg</sub>* for the discharging periods was calculated using the temperature data from the outer boreholes when fluid was injected in the outer boreholes and extracted from the center boreholes. The

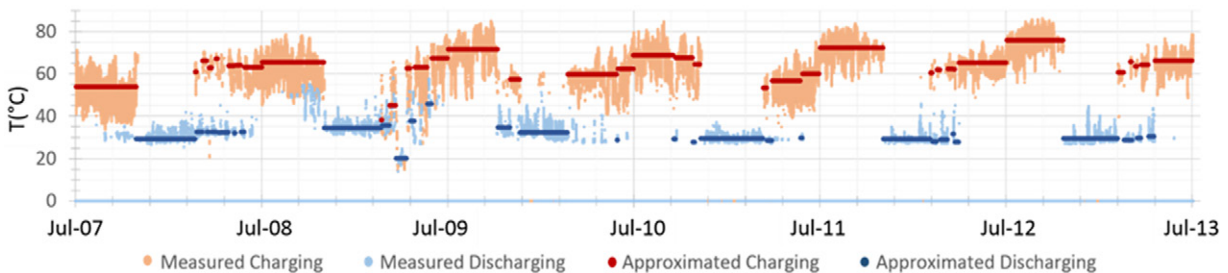


Fig. 4. Approximated simulation injection temperatures compared with the measured data for charging and discharging periods.

energy balance was accounted for through the flow rate calculation. The mass flow rate ( $q_j$ ) for each stress period was calculated as

$$q_i = \frac{J_i}{t_i c (T_{i\text{-avg in}} - T_{i\text{-avg out}})} \quad [5]$$

where  $t_i$  (s) is the length of the stress period,  $c$  is the specific heat of water ( $\text{J kg}^{-1} \text{ }^\circ\text{C}^{-1}$ ),  $T_{i\text{-avg in}}$  ( $^\circ\text{C}$ ) is the average injection temperature as calculated in Eq. [4], and  $T_{i\text{-avg out}}$  ( $^\circ\text{C}$ ) is the average extraction temperature for the stress period as calculated in Eq. [4];  $J_i$  is the total thermal energy injected during the given stress period, calculated by

$$J_i = J_t \frac{t_i}{t_t} \quad [6]$$

The total thermal energy in joules injected during charging stress periods (or total thermal energy in joules discharged during discharging stress periods) during the course of a year ( $J_t$ ) were divided into each stress period and weighted by the length of the stress period. Although the total energy calculation weighted by the length of the stress period may seem rough, it serves to maintain the total energy balance when incorporated into Eq. [5] because it accounts for the overestimated average charging temperatures and underestimated discharging temperatures in Eq. [4]. In Eq. [6],  $t_i$  is the length of the stress period and  $t_t$  is the total charging (or discharging) time for the year. Injection enthalpies are calculated by TOUGH2 from the steam table using average injection temperatures calculated in Eq. [4] and atmospheric pressure. Details of the injection scheme are listed in Supplemental Table S1.

The initial temperature was obtained through calibration by comparing modeled temperature to measured temperature data at the injection–extraction sites as well as each of the temperature sensor locations. Optimal results were obtained using an initial soil temperature of  $8.1^\circ\text{C}$ . An additional consideration is that the actual system was operational for about 3 mo from 12 April to 1 July before the start of data collection. These 3 mo generally correspond to charging periods of other operational years. This indicates that by the time data collection began, temperatures probably had already increased within the BTES subsurface area. To take this into consideration, the model was run for a 3-mo period utilizing the same injection temperature and flow rate as the first charging period. This 3-mo simulation yielded a simulated initial average core temperature around  $33^\circ\text{C}$ , which compared well with the measured data. The average core temperature was calculated using (Sibbitt et al., 2012)

$$T_c = \frac{T_t + 2T_m + T_b}{4} \quad [7]$$

where  $T_c$  is the weighted average core temperature,  $T_t$  is the BTES center top temperature (Sensor TS-22-1),  $T_m$  is the BTES center mid-height temperature (TS-22-4), and  $T_b$  is the BTES center bottom temperature (TS-22-7). Temperature sensor locations are

shown in Fig. 2. The soil was assumed to be saturated and thus the water table was assumed to be at the ground surface for simplicity. Hydrostatic pressure was assumed as an initial condition throughout the simulated domain. No background groundwater flow was assumed in the simulations.

## Model Results

The response of the BTES system from July 2007 to July 2013 was simulated. Heat flux ( $H$ ) into the subsurface for each time step can be calculated as

$$H = \frac{(T_{c_j} - T_{o_j}) Q_j c \rho}{2\pi R b B} \quad [8]$$

where  $T_{c_j}$  is the measured temperature at the center boreholes ( $^\circ\text{C}$ ),  $T_{o_j}$  is the measured temperature at the outer boreholes ( $^\circ\text{C}$ ),  $Q_j$  is the measured volumetric flow rate ( $\text{m}^3 \text{ s}^{-1}$ ),  $\Delta t_j$  is the  $j$ th time interval (s),  $c$  is the specific heat capacity of water ( $\text{J kg}^{-1} \text{ }^\circ\text{C}^{-1}$ ),  $\rho$  is the density of water ( $\text{kg m}^{-3}$ ),  $R$  is the borehole radius (m),  $b$  is the borehole height (m), and  $B$  is the number of boreholes. The average heat flux into the modeled BTES system at the DLSC was  $25 \text{ W m}^{-2}$ .

### Temperature Distribution in the Borehole Thermal Energy System at Drake Landing

The evolution of thermal storage plumes with time is shown in Fig. 5 for the borehole region at  $x = 6.5 \text{ m}$  and  $z = -17.5 \text{ m}$ . Modeled temperatures are shown for September corresponding to the end of the longest charging period and for March corresponding to the end of the longest discharging period. The radius of thermal contours at the depth of  $17.5 \text{ m}$  are shown in Supplemental Fig. S1.

Several observations can be made from these simulations. The borehole region shows a trend of increasing temperature with time (Fig. 5). By Year 6, average temperatures at all sensor locations were about  $20^\circ\text{C}$  higher than in Year 1. In the charging period of the first year (Fig. 5a and 5b), the elevated temperature region was restricted within the borehole region ( $x < 15 \text{ m}$ ,  $z < 40 \text{ m}$ ), reaching a maximum weighted core temperature of about  $52^\circ\text{C}$ . By the end of the discharging period (Fig. 5c and 5d), center temperatures decreased as some of the heat was extracted and some was conducted outward into the surrounding medium. As time elapsed, the elevated temperature region expanded both outward and downward. The maximum simulated weighted core temperature in the sixth year was about  $70^\circ\text{C}$ ,  $18^\circ\text{C}$  higher than that in the first year. Correspondingly, the minimum weighted core temperature in Year 6 was about  $48^\circ\text{C}$ , about  $19^\circ\text{C}$  warmer than that at the end of the discharging period in the first year.

Measured and simulated temperature profiles are shown in Fig. 6 for several locations including the center and outer boreholes, lateral sensors near the surface, and depth sensors near the center of

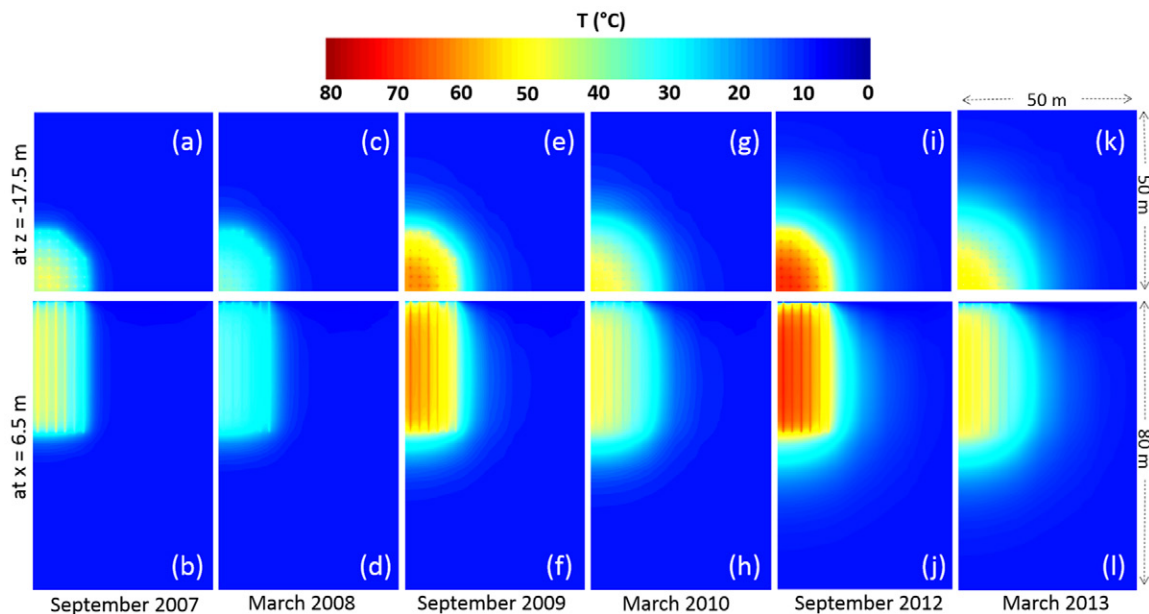


Fig. 5. Simulated temperature distribution at a depth of 17.5 m (upper) and a lateral cross-section located 6.5 m from the system's center (lower). Results are shown for the ends of the charging (a, b, e, f, i, and j) and discharging (c, d, g, h, k, and l) periods for early, middle, and late years of operation.

the system. The simulated temperatures at the center (Fig. 6a) and outer boreholes (Fig. 6b) represent the fluid injection and extraction temperatures. Approximated injection temperatures based on the measured data were imposed at the center boreholes during charging and at the outer boreholes during discharging periods. This allows comparison between the measured and simulated extraction temperatures at the outer boreholes during charging periods and the center boreholes during discharging periods. The simulated annual average extraction temperatures at the center boreholes ranged from 47.6 to 62.6°C. The simulated annual average extraction temperatures at the outer boreholes ranged from 30.0 to 41.2°C. The average simulated temperatures at the center boreholes were slightly above the average measured temperatures, with a maximum difference of 5.7°C. The average simulated temperatures at the outer boreholes were slightly below the average measured temperatures, with a maximum difference of 2.9°C.

Measured soil temperatures from several near-surface locations were compared with the simulated temperatures. Soil temperature profiles for two of these locations, one near the center boreholes (TS-24-2) and one near the outer edge of the borehole region (TS-24-7), are shown in Fig. 6c and 6d. The difference in simulated annual average temperature and measured temperature at the lateral temperature sensors ranged from 0.1 to 3.8°C. The largest discrepancy in each year was at Sensor TS-24-4, which lies in the middle of the borehole region, farthest from the injection–extraction sites. Simulated average annual simulated temperatures at the lateral sensors were slightly higher than those measured for all years.

Temperature sensors are used to continuously measure the subsurface temperature at different depths in the center of the BTES

system. The temperatures at two of these depths as a function of time are shown in Fig. 6e and 6f (temperatures at additional depths are detailed in Supplemental Fig. S2 and S3). These sensors represent depths near the top of the borehole region (TS-22-1) and at three quarters of the system's depth (TS-22-5). Several of the sensors failed before this simulation and were not available for comparison. While temperatures overall increased with time, the oscillating signal of the injection temperatures was dampened with depth. The difference in simulated and measured annual average temperatures at the sensor locations ranged from 0.7 to 4.0°C. Simulated temperatures were slightly higher than measured temperatures near the surface and slightly lower than measured at depth. The simulated temperature time series at depth also shows smaller oscillating amplitude than the measured oscillations, as well as a slight delay in peak temperatures. These discrepancies may be a result of the assumed homogeneity of soil parameters with depth while the actual subsurface is probably heterogeneous. For example, the soil thermal conductivity may differ with geological layering. Although the homogeneous thermal conductivity model appropriately replicated the average injection, extraction, and core temperatures, actual conductivity may vary with depth, thus affecting the distribution of the thermal plume.

The largest discrepancies between the measured and simulated temperatures occurred when there were frequent alternations between charging and discharging. These simulation periods correspond to the time periods when the flow direction changed frequently, sometimes multiple times in a day. This frequent change of flow direction is smoothed out in the model (Fig. 4) and could lead to the discrepancies during these periods.



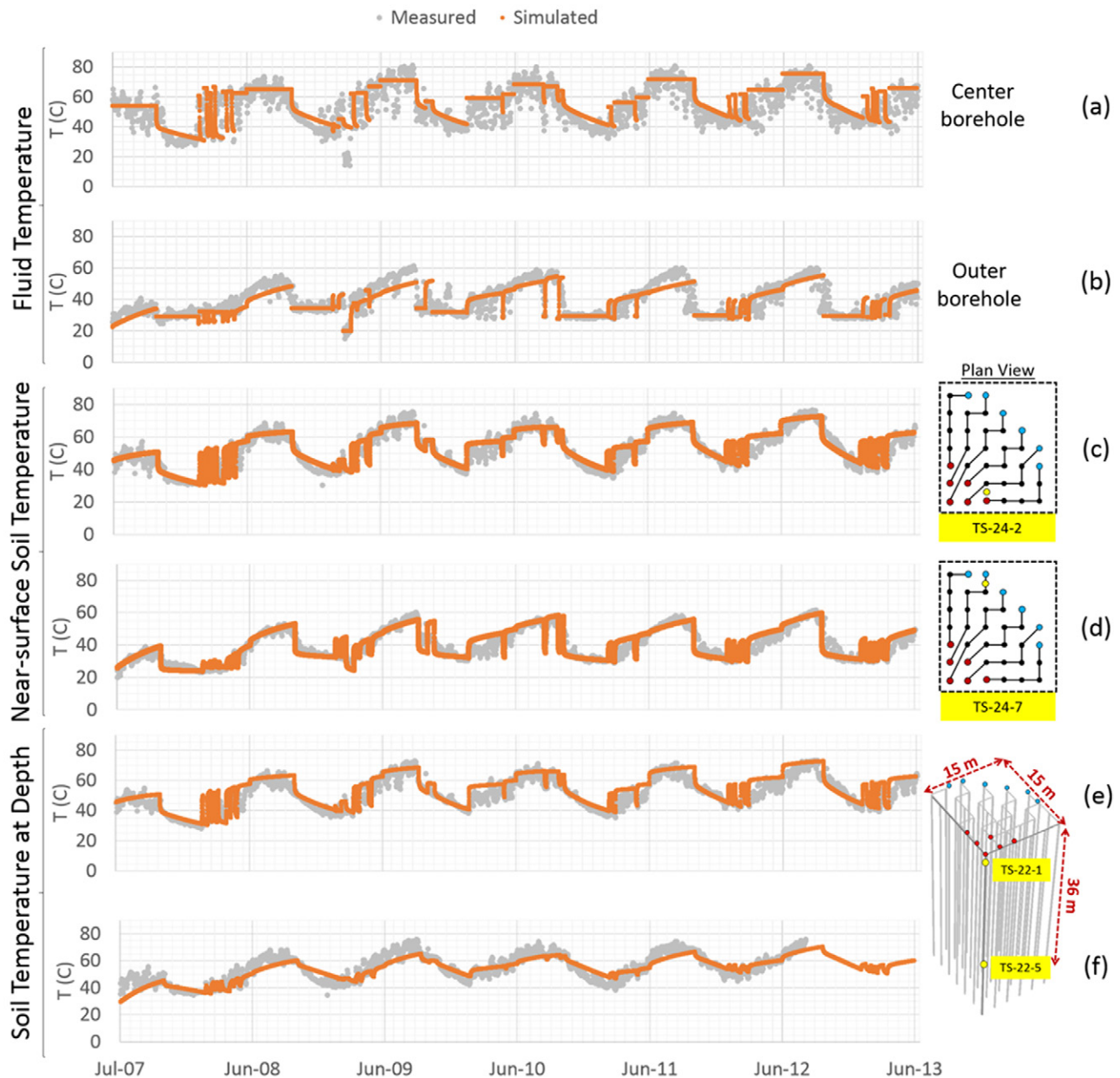


Fig. 6. Comparison of simulated and daily average measured temperature profiles at key locations including the averaged (a) center and (b) outer boreholes, (c,d) lateral sensors near the surface, and (e,f) depth sensors near the center of the system. Temperature sensor locations are shown as yellow circles, red circles indicate center boreholes, and blue circles indicate outer boreholes. Sensor TS-22-5 failed by September 2012.

Overall, the simulated temperatures at the sensor locations closely resemble the daily average measured temperatures at the corresponding locations. This suggests that the method of averaging flow rate and temperature while preserving total energy input properly replicates the system behavior. The model sufficiently approximated heat transport and storage in the BTES system at the DLSC and provides a solid basis for future study of factors affecting BTES system performance.

### Heat Extraction Efficiency at Drake Landing

The annual heat extraction efficiency for the 6 yr of simulation were calculated according to Eq. [1] and plotted in Fig. 7. The

simulated efficiencies from Years 1 to 6 are 5.2, 20.6, 35.3, 54.5, 31.1, and 48.7%, respectively. These values closely mirror the rise and fall of the measured efficiencies. The annual heat extraction efficiency generally increases with time, with the exception of Year 5. It is believed that efficiency in Year 5 was lower than the previous year due to the high amount of energy extracted and lower amount of solar thermal energy injected into the system in Year 4. This resulted in a smaller thermal plume and less available energy for extraction at the start of Year 5. It should also be noted that the maximum efficiencies are much higher than those reported by Zhang et al. (2012). This is because their estimates used an annually repeated injection scheme derived from the first year of

injection data, whereas this model considered the actual energy inputs from 2007 through 2013.

Heat transport and storage processes in the BTES system can be further dissected through examining the thermal energy distribution in terms of heat injected, heat recovered, heat stored in the borehole region, and heat lost from the borehole region. The heat loss decreased with time as the system became able to more efficiently recover thermal energy, but there is always heat loss into the surrounding porous media because there is heat flow directed away from the borehole region even during the discharging months (Supplemental Fig. S4). After 6 yr, 31.5% of the heat injected into the system was recovered in total, 21.9% remained in the borehole region, and 46.7% escaped the borehole region (Supplemental Fig. S5). After the first year, the cumulative percentage of heat leaving the borehole region remained relatively constant. The fraction of energy stored in the region decreased with time while the energy extracted increased with time, approaching a steady state and reflecting the increase in efficiency.

## 💧 Sensitivity Analyses

Because available solar energy and input temperatures vary from year to year, it is difficult to predict the long-term heat extraction efficiency of this particular system; however, general trends in long-term efficiency can be examined using a simplified model with an annual repeating injection cycle. The simplified model can be used to quantitatively examine the controlling factors on long-term BTES system efficiency such as the soil and rock hydrological and thermal properties. Sensitivity analyses are used to understand how different geological settings may influence BTES heat extraction efficiency. Through sensitivity study, the role of soil thermal conductivity, background hydraulic gradient, soil permeability, and soil saturation in BTES systems can be assessed. Most previous models have assumed saturated conditions, but BTES systems are probably located in unsaturated zones. Thus it is important to examine the role of saturation in the thermal energy storage and recovery processes.

The sensitivity of BTES system heat extraction efficiency to soil thermal and hydrological parameters was examined using a simplified model for computational efficiency. The simplified model contained two boreholes and an annually repeating injection scheme. The background soil temperature was set to 15°C. All other parameters were taken from the DLSC model. Two boreholes were simulated with a plane of symmetry next to the center borehole. The domain had dimensions of 100 m long by 50 m wide by 50 m deep. Each U-tube pipe was 30 m deep, with a separation of 5 m between the two U-tubes. The simulated domain was discretized by 38 varying-space grids in the  $x$  direction, 43 in the

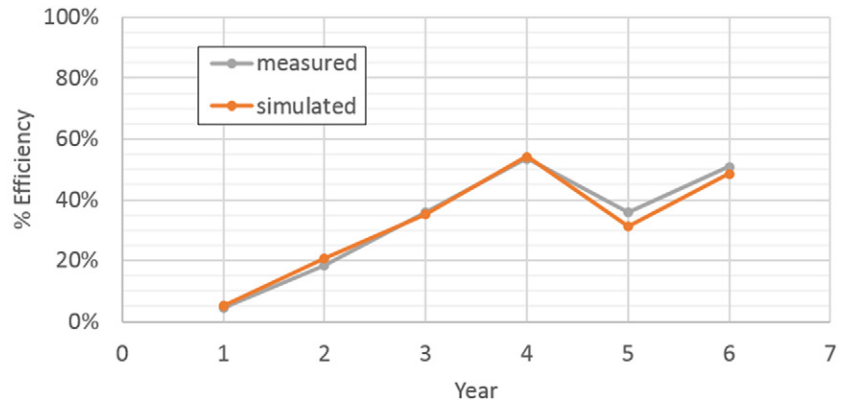


Fig. 7. Simulated and measured borehole thermal energy storage heat extraction efficiency for the first 6 yr of operation at Drake Landing. Simulated efficiencies are within 5% of those measured.

$y$  direction, and 41 in the  $z$  direction. The discretization of the domain and the imposed boundary conditions are shown in Fig. 8a. Placement of the U-tube pipes in relation to the domain are shown in Fig. 8b.

A simple annually repeating injection scheme was imposed, with 8 mo of charging at 60°C followed by 4 mo of discharging at 30°C. These temperatures are close to the average injection temperatures at the DLSC site. The length of the charging period was exaggerated to obtain a sizable heat storage plume in the simplified system containing only two boreholes. Thus, the sensitivity results are not intended to portray realistic BTES system numbers but rather to demonstrate how a range in soil hydrologic and thermal properties affects system performance.

A base scenario assumed that the subsurface has homogeneous and isotropic soil similar to the DLSC site and no background groundwater flow. In the sensitivity analyses, the following properties were systematically altered to observe their effect on BTES system performance: soil thermal conductivity, groundwater flow, and soil permeability. All material properties and boundary conditions were maintained with the exception of the variable of interest in each analysis. All sensitivity analyses were conducted under saturated conditions. An additional set of soil permeability sensitivity analyses was conducted under unsaturated conditions as described below. All analyzed variables and their ranges are presented in Table 2. Heat flux into the subsurface was calculated according to Eq. [8]. The average heat flux into the system for the simplified model ranged from 20 to 50 W m<sup>-2</sup> depending on the parameter scenarios.

## 💧 Sensitivity Results

### Baseline Scenario

The baseline scenario for the simplified model used the same parameters from the DLSC model except the new simplified

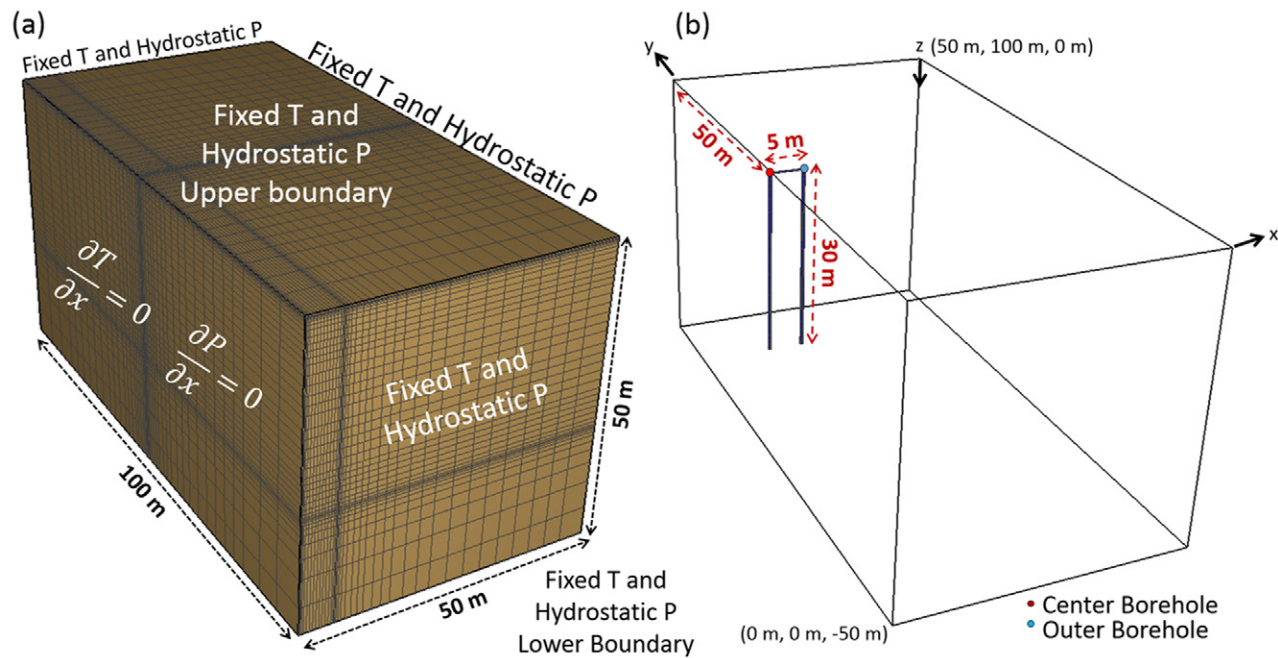


Fig. 8. (a) Simplified model dimensions and boundary temperature ( $T$ ) and hydrostatic pressure ( $P$ ) conditions; and (b) location and dimensions of piping and temperature sensors within the model domain.

annually repeating injection scheme. The base scenario model was run for 20 yr to observe long-term trends in heat extraction efficiency. The simulation results show efficiency starting at 13.3% for the first year and increasing rapidly in the following few years. The efficiency asymptotically approached a steady-state value of 22.9% by about Year 6 (Fig. 9). The efficiency represents the proportional amount of energy recovered by the system each year. The amount of energy into the system, calculated as in Eq. [3], decreased with time toward a steady state. This can be explained by the decrease in the thermal gradient between the U-tube piping and soil as the thermal storage plume developed. The amount that can be extracted, calculated as in Eq. [2], increased with time toward a steady state. This can similarly be explained by an increase in the thermal gradient in the discharging months as the thermal plume developed and temperatures in the borehole area increased compared with the circulating fluid.

Table 2. Parameters examined in the sensitivity analyses and their range of values. Relative permeability for unsaturated soils varies according to the van Genuchten–Mualem model where  $m$ , the dimensionless van Genuchten parameter based on soil water retention = 0.5 and  $P_0$ , which is related to the air-entry pressure = 0.1 Pa. Equations are given in the supplement.

Parameter	Lower limit	Upper limit
Fluid circulation rate, $\text{kg s}^{-1}$	0.05	0.5
Soil thermal conductivity, $\text{W m}^{-1} \text{ }^\circ\text{C}^{-1}$	0.5	3.0
Hydraulic gradient	0	0.05
Saturated soil intrinsic permeability, $\text{m}^2$	$1.5 \times 10^{-18}$	$1.5 \times 10^{-6}$
Unsaturated soil intrinsic permeability, $\text{m}^2$	$1.5 \times 10^{-18}$	$1.5 \times 10^{-6}$

These results suggest that with a given set of base scenario parameters, there exists an upper limit steady-state heat extraction efficiency. The steady-state efficiency of the simplified system was lower than that of the BTES system at the DLSC due to the inclusion of fewer boreholes and a different injection scheme. Efficiencies obtained from sensitivity analyses are compared with the base scenario.

## Thermal Conductivity

It has been observed that thermal conductivity is influenced by mineralogy, rock density, degree of saturation, and temperature (Farouki 1981; Brandon and Mitchell, 1989; Smits et al., 2013). Heat conduction is more robust at higher thermal conductivities, but the rate for heat conduction away from a reservoir also increases. Thus, it has been suggested that medium thermal conductivities may be desirable for thermal energy storage systems (Socaciu, 2011; Başer and McCartney, 2015).

A range of soil thermal conductivity values from 0.5 to 3  $\text{W m}^{-1} \text{ }^\circ\text{C}^{-1}$  was considered. The results show that BTES heat extraction efficiency decreases with increasing soil thermal conductivity (Fig. 10). A soil with a low thermal conductivity of 0.5  $\text{W m}^{-1} \text{ }^\circ\text{C}^{-1}$  showed 47% higher efficiency in the first year than the base scenario, with a thermal conductivity of 2.0  $\text{W m}^{-1} \text{ }^\circ\text{C}^{-1}$ . Energy injection into the soil decreases for lower soil thermal conductivity values, but the ability to extract energy showed slight increases. The development of the thermal plume for low and high thermal conductivity soils is shown in Fig. 11. In both cases, the thermal plume grew outward despite the system being in a heat discharging state. Heat transport away from the piping is always at play

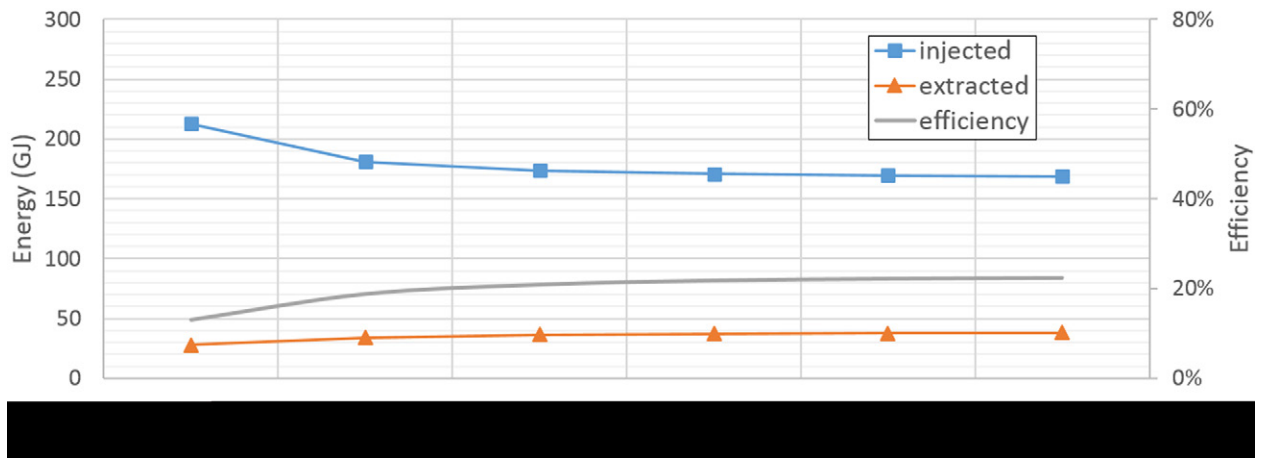


Fig. 9. Simulated energy injection and extraction and heat extraction efficiency of the modeled borehole thermal energy storage system base scenario with time.

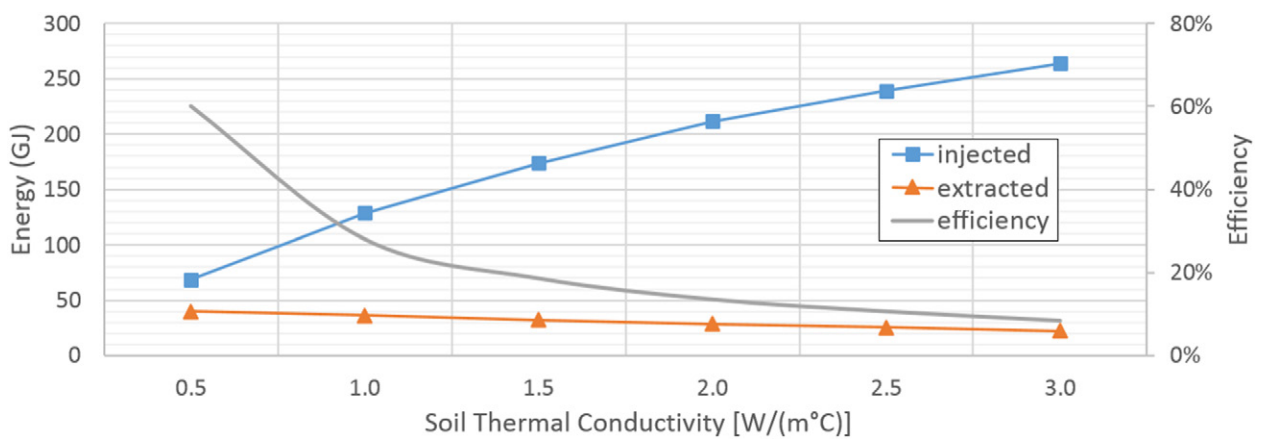


Fig. 10. Simulated energy injection and withdrawal and heat extraction efficiency of the borehole thermal energy storage system at various soil thermal conductivity values.

as long as there is a thermal gradient between the plume and the surrounding medium to drive conduction. In the case with higher soil thermal conductivity ( $3.0 \text{ W m}^{-1} \text{ }^\circ\text{C}^{-1}$ ), a much larger thermal plume resulted from the increased ability to receive injected energy and conduct the heat into the surrounding soil in the charging phase. This increased ability of the heat to move outward away from the pipes resulted in lower temperatures near the pipes (about  $52.5^\circ\text{C}$ ) and thus a lower gradient for heat to flow back toward the piping in the discharge phase. At the end of charging in the low-conductivity case, higher temperatures remained near the pipes (about  $55.5^\circ\text{C}$ ), creating a higher gradient to drive heat flow back toward the piping in the discharging phase. The higher gradient in the low-conductivity case allowed a greater portion of the heat to be recovered, whereas in the high-conductivity case, the thermal plume continued to expand outward.

These results suggest that the thermal properties of the subsurface play a significant role in the heat extraction efficiency of BTES systems. Low thermal conductivity soils allow higher temperature gradients in the discharging phase and thus higher system

efficiency. Presently, only large-scale geothermal systems conduct regular thermal response tests to determine the effective thermal conductivity of the subsurface (Stauffer et al., 2013). Proper knowledge of soil thermal conductivity is essential for suitable emplacement and design of BTES systems.

### Groundwater Flow

In saturated systems, a background hydraulic gradient and therefore a groundwater flow field may exist. A test of this background groundwater flow influence on BTES heat extraction efficiency was conducted by incorporating a hydraulic gradient of 0.05, corresponding to a groundwater velocity of  $3.6 \times 10^{-8} \text{ m s}^{-1}$ . The result showed significant alteration of the thermal plume. A cross-section of the thermal plume after 1 yr is shown in Fig. 12 for the base scenario and the groundwater-flow scenario. The base scenario produced a thermal plume that symmetrically surrounded the piping area. When groundwater flow was incorporated, the thermal plume migrated in the direction of groundwater movement. This relatively small addition of groundwater movement resulted in a decrease in efficiency of 0.6% for the first year of

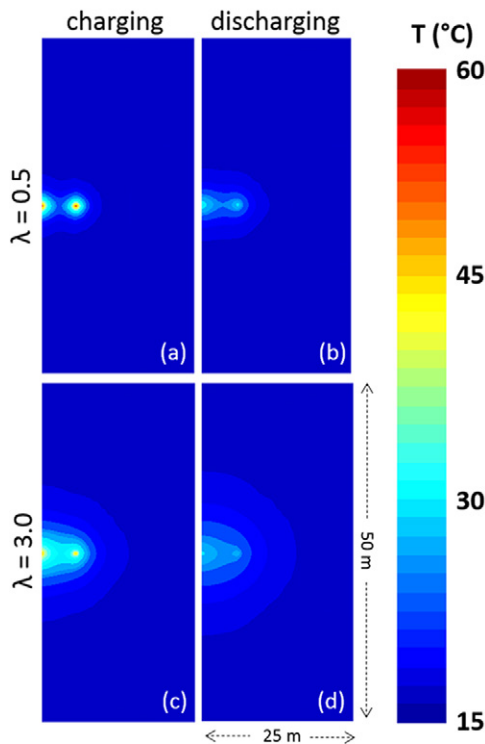


Fig. 11. Thermal plume development in soil with a thermal conductivity ( $\lambda$ ) of  $0.5 \text{ W m}^{-1} \text{ }^\circ\text{C}^{-1}$  (a) after a charging period and (b) after a discharging period and in soil with  $\lambda = 3.0 \text{ W m}^{-1} \text{ }^\circ\text{C}^{-1}$  (c) after a charging period and (d) after a discharging period. Cross-sections are located at  $z = -15 \text{ m}$ .

operation. This is because groundwater flow promotes heat advection and carries heat away from the BTES area, whereas in the base scenario, conduction is the primary means of heat transfer. Because greater hydraulic gradients would cause increased advection away from the BTES area, one can infer that BTES system areas of appreciable background hydraulic gradient would have

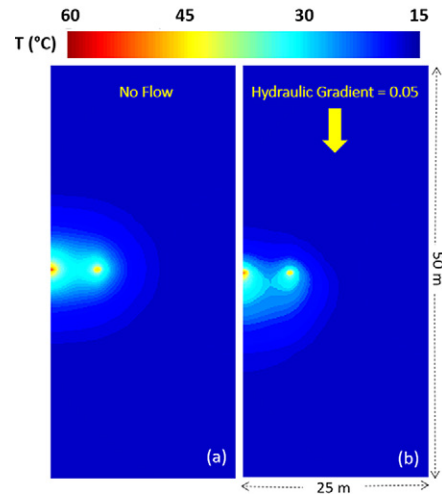


Fig. 12. Distribution of the thermal plume after 1 yr of simulation time at  $z = -15 \text{ m}$  with (a) no background hydraulic gradient and (b) a gradient of 0.05.

lower system efficiencies. These results indicate that groundwater flow has a limited influence on BTES performance for the given small hydraulic gradient in this case. The significance of groundwater flow influence under a higher hydraulic gradient warrants further study through examining the relative magnitude of heat conduction and heat convection.

### Soil Permeability

Heat extraction efficiencies varying with intrinsic soil permeability are shown in Fig. 13. Efficiency is maximized and relatively constant at permeability values of  $1.5 \times 10^{-12} \text{ m}^2$  and below. A decrease in efficiency occurs at permeability values  $>1.5 \times 10^{-12} \text{ m}^2$ . This phenomenon corresponds to when the dimensionless Rayleigh number ( $Ra$ ) is higher than a critical Rayleigh value ( $Ra_c$ ) of  $4\pi^2$  (Nield and Bejan, 1992). The Rayleigh number is calculated as

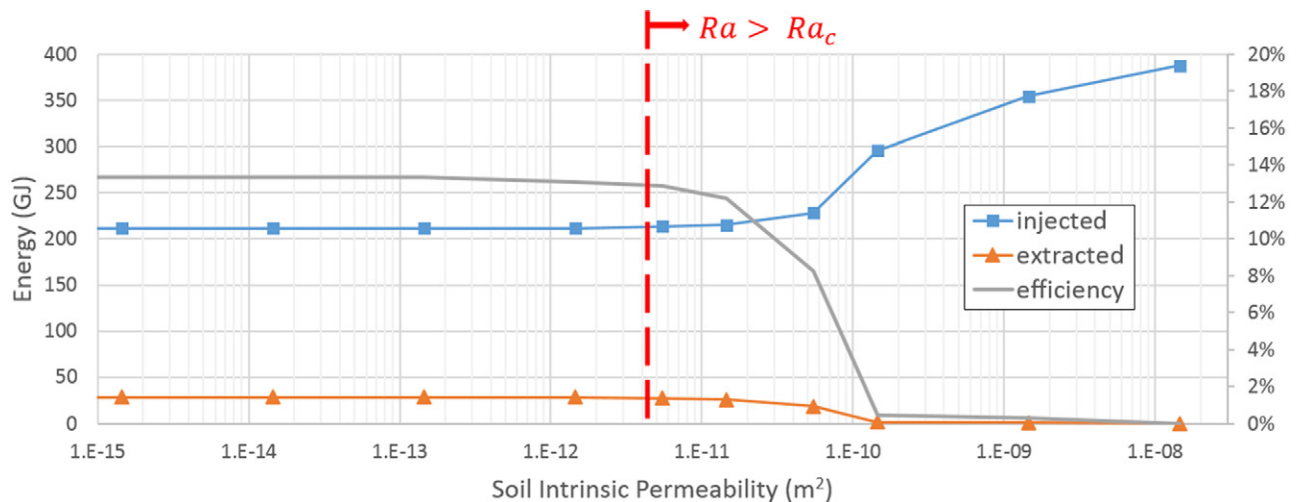


Fig. 13. Simulated energy injection and extraction and heat extraction efficiency of the borehole thermal energy storage system at various soil intrinsic permeability values. The red line indicates the permeability values for which the calculated two-dimensional Rayleigh number ( $Ra$ ) exceeds the critical Rayleigh value ( $Ra_c$ ).

$$Ra = \frac{L\alpha g k (T_s - T_\infty)}{\vartheta_1 \lambda} \quad [9]$$

where  $L$  is the length of the pipe (add units to all the variables and make sure they balance),  $\alpha$  is the thermal expansion coefficient of water,  $g$  is gravitational acceleration,  $k$  is horizontal permeability,  $T_s$  is temperature of the pipe wall,  $T_\infty$  is the background temperature,  $\vartheta_1$  is the kinematic viscosity of water, and  $\lambda$  is the effective thermal conductivity of the porous medium.

When a Rayleigh number exceeds the critical value, the onset of convection in a porous medium occurs. The thermal plume development and heat flow in a cross-section through the piping area for permeability values corresponding to Rayleigh numbers that fall above and below the critical Rayleigh value are shown in Fig. 14. Conduction is the dominant mode of heat transfer for the lower permeability values. The vectors show the flow of heat ( $\text{W m}^{-2}$ ) and support the presence of convection at Rayleigh numbers surpassing the critical value. For this system, the Rayleigh number exceeded the critical value, leading to convection, for soil permeability  $>1.5 \times 10^{-12} \text{ m}^2$ . At Rayleigh numbers slightly higher than the critical value, heat convection starts outside the borehole region (Fig. 14b). At even higher Rayleigh numbers, significant convection occurs outside the borehole region (Fig. 14c). This convective process is accompanied by lateral heat loss and a sharp decrease in system efficiency. A synthesis plot of Rayleigh numbers for differing permeability values is shown in the Supplemental Fig. S6.

After the onset of convection at soil permeability  $>1.5 \times 10^{-12} \text{ m}^2$ , the amount of energy into the system increases and the amount of energy extracted decreases (Fig. 13). The rate of heat transfer into the soil increases because the convective processes maintain a high temperature gradient away from the pipe. The convective processes effectively carry heat upward and away from the piping, creating

an asymmetric thermal plume. The system is unable to extract the heat as efficiently as in cases of little convection.

These model results suggest that low-permeability soils are preferable for enhancing the efficiency of BTES systems in saturated soil layers. Heat losses due to convection away from the piping area in high-permeability soils outweigh the potential benefits of convection occurring within the piping region. Future studies should consider different engineering layouts that may utilize convective processes in a more productive manner. For example, a greater distance between the boreholes may allow increased extraction temperatures associated with higher convection-induced temperature gradients within the borehole array itself. Another potential scenario might be to incorporate vertical subsurface thermal barriers surrounding the storage region to reduce lateral convective heat losses.

### Unsaturated Soil Permeability

Borehole thermal energy storage systems are probably located in unsaturated zones, in part to take advantage of the lower thermal conductivity with degree of saturation (Smits et al., 2013). It has been suggested that heat convection within the piping area may affect the performance of BTES systems in terms of both heat storage and the rate of heat transfer (McCartney et al., 2013). Lu (2001) found that the rate of heat transfer in a convective cell in an unsaturated soil layer may be up to 10 times faster than heat transfer by conduction. Previously, the influence of the soil intrinsic permeability on convective processes within a BTES system in saturated soil was shown. Here, the sensitivity of the BTES model to soil permeability and thermal conductivity in an unsaturated soil was examined.

To model the effect of an unsaturated soil setting, the simplified model was initialized with 25% liquid saturation in the upper 30 m and run to hydrostatic equilibrium before the transient simulation.

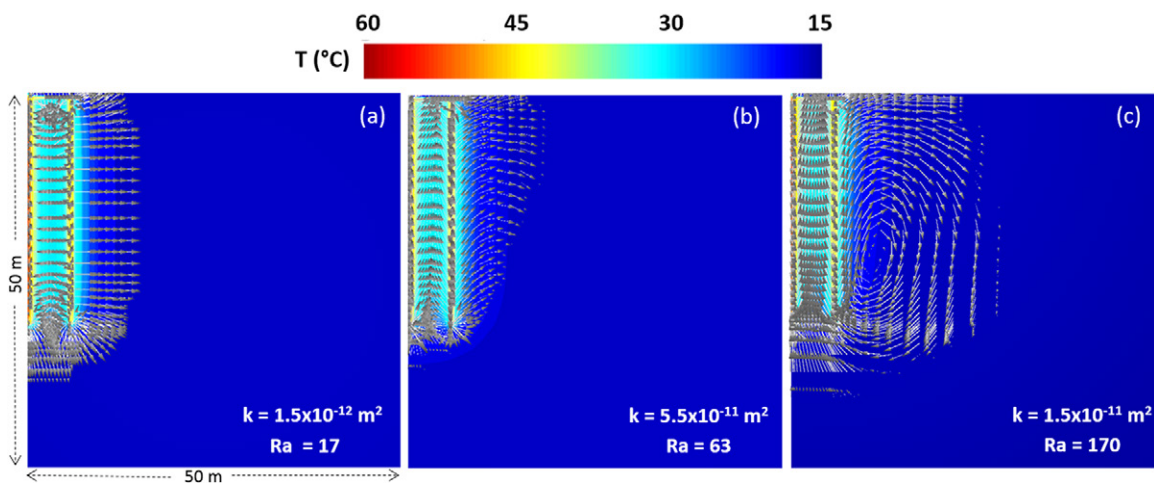


Fig. 14. Cross-sections through the piping area ( $y = 50 \text{ m}$ ) showing thermal plume development and heat flow during the charging phase of the saturated simulation for soil intrinsic permeability ( $k$ ) values corresponding to a Rayleigh number ( $Ra$ ) (a) below the critical Rayleigh value, (b) slightly above the critical Rayleigh value, and (c) significantly above the critical Rayleigh value. Vectors show flow of heat  $>1 \text{ W m}^{-2}$ .

The relative permeability of liquid water in the unsaturated case varies with the liquid degree of saturation. A van Genuchten–Mualem model (Mualem, 1976; van Genuchten, 1980) for relative permeability and soil water retention was used (details are shown in the supplement, Supplemental Fig. S7 and S8). We chose water retention properties representative of a sandy soil (air-entry capillary pressure of 0.1 Pa), although future studies may look at varying this parameter for different soil types. As the degree of saturation increases, the liquid-phase permeability dominates, while at low saturation the gas-phase permeability dominates.

Thermal conductivity also varies with the liquid degree of saturation. In TOUGH2, the effective thermal conductivity ( $\lambda$ ) is calculated as

$$\lambda = \lambda_D + \sqrt{S_l} (\lambda_w - \lambda_D) \quad [10]$$

where  $\lambda_D$  is the dry soil conductivity,  $S_l$  is the liquid saturation, and  $\lambda_w$  is the saturated wet soil conductivity. Wet and dry thermal conductivity values are calculated as (Newson and O’Sullivan, 2004)

$$\lambda_w = (1-n)\lambda_{\text{soil}} + n\lambda_{\text{water}} \quad [11]$$

and

$$\lambda_D = (1-n)\lambda_{\text{soil}} + n\lambda_{\text{air}} \quad [12]$$

where  $n$  is porosity,  $\lambda_{\text{soil}}$  is the thermal conductivity of soil grains,  $\lambda_{\text{water}}$  is the thermal conductivity of water, and  $\lambda_{\text{air}}$  is the thermal conductivity of air. In this study,  $0.654 \text{ W m}^{-1} \text{ }^\circ\text{C}^{-1}$  was used for the thermal conductivity of water at  $20^\circ\text{C}$ , and  $0.029 \text{ W m}^{-1} \text{ }^\circ\text{C}^{-1}$  was used for the thermal conductivity of air at  $60^\circ\text{C}$ . A range of soil thermal conductivity from  $0.5$  to  $3 \text{ W m}^{-1} \text{ }^\circ\text{C}^{-1}$  was modeled.

The unsaturated soil modeling intended to address the following specific questions: How does the heat extraction efficiency of the unsaturated system compare with the saturated case for similar intrinsic permeability values? How does the onset of convection differ in the unsaturated and saturated cases? How does convection affect the BTES system heat extraction efficiency?

Heat extraction efficiency at various intrinsic soil permeability values in the unsaturated model is shown in Fig. 15. Similar to the saturated case, efficiency was maximized and stayed constant at low permeability values and then sharply decreased at higher values. In the unsaturated model, this decrease occurred at an intrinsic permeability of  $1.5 \times 10^{-9} \text{ m}^2$ , corresponding to a relative water permeability of  $9.2 \times 10^{-15} \text{ m}^2$  based on the van Genuchten relative permeability curve used. The phenomenon also corresponds to a dimensionless Rayleigh number ( $Ra$ ) higher than the critical Rayleigh number ( $Ra_c$ ) of  $4\pi^2$ . For the unsaturated soil case, the Rayleigh number was calculated according to Amili and Yortsos (2004):

$$Ra = \frac{C_v L k g (\rho_l - \rho_v)}{\vartheta_v \lambda} \quad [13]$$

where  $C_v$  is the specific heat capacity of vapor ( $\text{J kg}^{-1} \text{ }^\circ\text{C}^{-1}$ ),  $L$  is the length of the pipe (m),  $g$  is the gravitational acceleration ( $\text{m s}^{-2}$ ),  $k$  is horizontal permeability ( $\text{m}^2$ ),  $\rho_l$  is density of the liquid ( $\text{kg m}^{-3}$ ),  $\rho_v$  is the density of water vapor ( $\text{kg m}^{-3}$ ),  $\vartheta_v$  is kinematic viscosity of water vapor ( $\text{Pa s}$ ), and  $\lambda$  is the effective thermal conductivity of the porous medium ( $\text{W m}^{-1} \text{ }^\circ\text{C}^{-1}$ ).

As in the saturated soil case, conduction appears to be the dominant mode of heat transfer for the lower permeability values, while convection occurs in higher permeability soils. Figure 16 shows the thermal plume development and heat flow in a

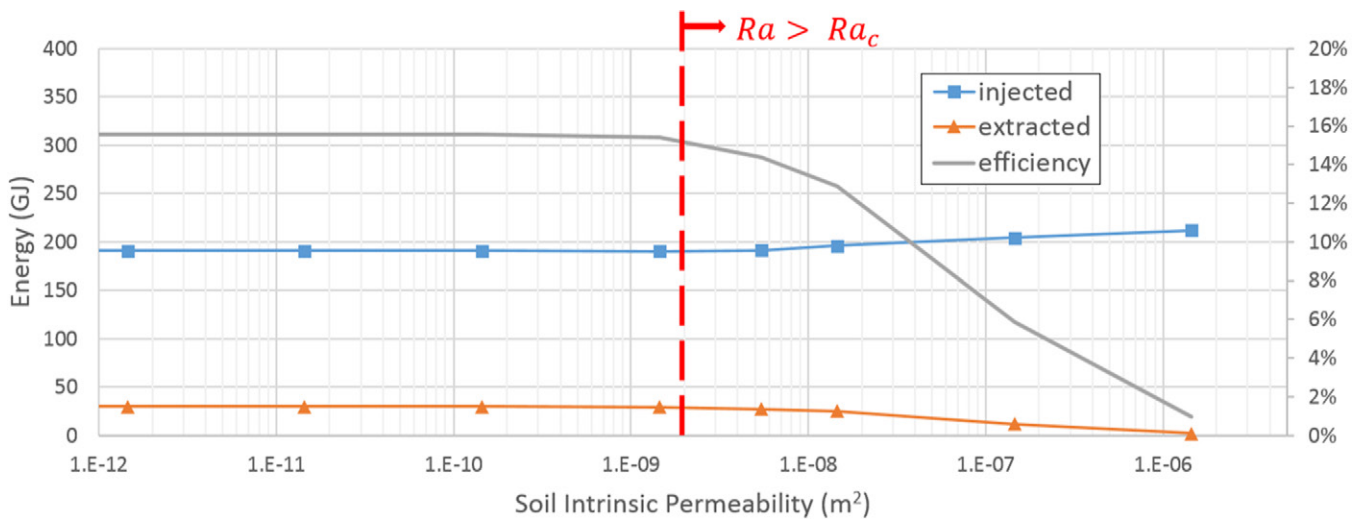


Fig. 15. Simulated energy injection and extraction and heat extraction efficiency of the borehole thermal energy storage system at various soil intrinsic permeability values in the unsaturated model. The red line indicates the permeability values for which the calculated two-dimensional Rayleigh number ( $Ra$ ) exceeds the critical Rayleigh value ( $Ra_c$ ).

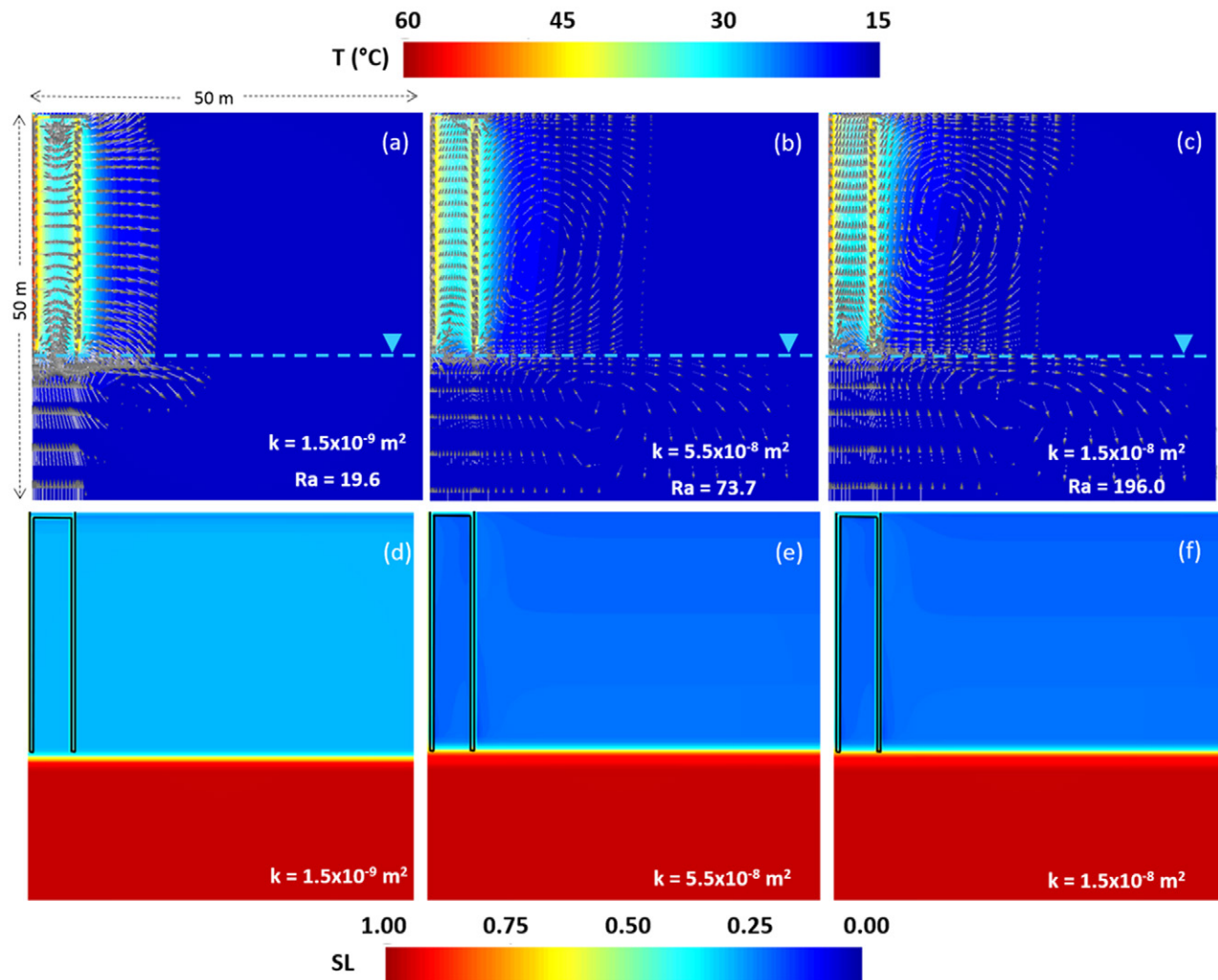


Fig. 16. Cross-sections through the piping area ( $y = 50 \text{ m}$ ) showing (a,b,c) thermal plume development and heat flow, and (d,e,f) degree of saturation of liquid (SL) during the charging phase of the unsaturated simulation for soil intrinsic permeability ( $k$ ) values corresponding to a Rayleigh number (a,d) below the critical Rayleigh value, (b,e) slightly above the critical Rayleigh value, and (c,f) significantly above the critical Rayleigh value. Vectors show flow of heat  $>1 \text{ W m}^{-2}$ .

cross-section through the piping area for permeability values corresponding to Rayleigh numbers that fall above and below the critical Rayleigh value. The heat flow vectors demonstrate the presence of convective processes in the unsaturated zone at higher Rayleigh values. Here, the Rayleigh number exceeded the critical value for soils with intrinsic permeability  $>1.5 \times 10^{-9} \text{ m}^2$ . Convection contributes to lateral heat loss and correlates to the decrease in efficiency shown in Fig. 15. A synthesis plot of Rayleigh numbers for differing permeability values is shown in Supplemental Fig. S6.

After the onset of convection in soils with intrinsic permeability  $>1.5 \times 10^{-9} \text{ m}^2$ , the amount of energy into the system increased and the amount of energy recovered decreased (Fig. 15). As in the saturated case, the rate of heat transfer into the soil increased because the convective processes maintained a high temperature gradient away from the pipe. Convective processes carry heat

upward and away from the piping, creating an asymmetric thermal plume and an associated decrease in efficiency.

The unsaturated soil produced higher energy outputs than the saturated case for an intrinsic soil permeability between  $1.5 \times 10^{-12}$  and  $1.5 \times 10^{-9} \text{ m}^2$  due to the delayed onset of convection in the unsaturated scenario. An unsaturated soil will have a lower effective permeability than its intrinsic permeability because the connection between pores is decreased when less water is available. The low permeability hinders potential convective processes that would otherwise occur in the saturated case. Thus, if the subsurface has a permeability in the range of  $1.5 \times 10^{-12}$  and  $1.5 \times 10^{-9} \text{ m}^2$ , an unsaturated soil is desirable because it will allow heat transfer by conduction rather than convection and the system will run efficiently. Energy output is maximized in low-permeability soils. For soil permeability  $<1.5 \times 10^{-12} \text{ m}^2$ , either a saturated or unsaturated subsurface will produce similar energy



output. Finally, if the soil permeability is  $>1.5 \times 10^{-9} \text{ m}^2$ , neither a saturated nor unsaturated subsurface will produce a strong energy output due to the dominance of convective heat transfer.

The overall heat extraction efficiency is higher in the unsaturated system than that of the saturated system for all permeability values. Specifically, in the unsaturated case, a higher proportion of the injected heat can be recovered. To explain this, one can look to thermal conductivity, which varies with saturation. Lower saturation corresponds to lower thermal conductivity because air makes up a great portion of the void space. The rate of radial heat loss may be lower due to air's insulating effect. As was shown in the thermal conductivity analysis, a lower thermal conductivity leads to greater energy recovery due to the distribution of the thermal gradients during the charging and discharging phases. The total amount of energy stored in the unsaturated system is also higher than that of the saturated system.

Saturation and permeability were shown to play a large role in BTES system heat extraction efficiency. In both the saturated and unsaturated models, low-permeability soils allowed a higher BTES system efficiency. In high-permeability soils, both saturated and unsaturated systems showed decreased efficiency from convective heat loss. Finally, the overall heat extraction efficiency of unsaturated systems at all permeability values was shown to be higher than for saturated systems due to lower effective thermal conductivity.

## Summary and Concluding Remarks

A three-dimensional transient fluid flow and heat transfer model for the subsurface BTES system at the DLSC was established using TOUGH2. The model used the time-dependent injection temperatures and energy input measured at the site. A total of 6 yr of annual cycles were simulated from July 2007 through July 2013. The modeled time-dependent temperatures within the borehole region agreed well with the measured values. The model sufficiently replicated the BTES system behavior at the DLSC and provides the basis for future study of factors affecting BTES system performance. The model confirmed a trend of increasing BTES system heat extraction efficiency with time toward a steady state. Heat flow out from the borehole region decreased due to a decreasing thermal gradient, thus more thermal energy was recovered as a result. However, as long as there is a thermal gradient between the thermal storage plume and its surroundings, there will always be some heat loss into the surroundings.

Sensitivity analyses were performed to quantitatively examine how soil hydrological and thermal properties affect BTES system performance. The examined parameters included soil thermal conductivity, hydraulic gradient, and soil permeability under both

saturated and unsaturated conditions. Sensitivity analyses led to the following conclusions:

1. The BTES system heat extraction efficiency increases with decreasing soil thermal conductivity. Low-conductivity soils allow more concentrated thermal plumes and thus higher temperature gradients near the pipes during the discharging phase. The higher gradients allow a greater portion of thermal energy to be recovered in the winter months and therefore yield higher system efficiency.
2. The BTES system heat extraction efficiency decreases with the presence of regional groundwater flow. When a hydraulic gradient is incorporated, advective processes can cause the thermal plume to migrate in the direction of groundwater movement. This leads to less thermal energy availability near the piping during the recovery phase and an associated decrease in system efficiency.
3. The BTES system heat extraction efficiency decreases with convective heat losses associated with high soil permeability for both saturated and unsaturated soils. The high permeability allows convective processes to carry heat upward and away from the piping.
4. Saturation was shown to affect the BTES system heat extraction efficiency in two primary ways. First, convection onset occurs at higher intrinsic permeability values in unsaturated soils than saturated soils. This is a product of the influence of water content on the relative permeability of the soil. Lower relative permeability in unsaturated soils hinders the convective processes below a critical threshold intrinsic permeability, leading to higher efficiencies than for saturated soils. Second, the overall heat extraction efficiency of unsaturated systems at all permeability values was shown to be higher than for saturated systems due to the insulating effect of air and a lower effective thermal conductivity.

Insights gained from this model study suggest that site-specific characteristics of the subsurface deserve greater consideration in the planning and design of underground thermal energy storage systems. Based on the sensitivity analyses, a desirable geological setting for BTES systems should consist of low thermal conductivity soils, a low hydraulic gradient, low intrinsic permeability, and low saturation vadose zones. The role of convective processes may be further explored to increase the heat extraction efficiency if they can be confined within the piping region.

## Acknowledgments

We would like to thank Bill Wong of Leidos Canada and Bruce Sibbitt from NRC Canada for sharing the data from DLSC. We also thank Ning Lu and Rong Lei Zhong for initial discussions on TOUGH2 modeling. Funding from NSF Grant CMMI 1230237 is greatly appreciated. The views in this paper are those of the authors alone.

## References

- Acuna, J., and B. Palm. 2013. Distributed thermal response tests on pipe-in-pipe borehole heat exchangers. *Appl. Energy* 109:312–320. doi:10.1016/j.apenergy.2013.01.024
- Amili, P., and Y. Yortsos. 2004. Stability of heat pipes in vapor-dominated systems. *Int. J. Heat Mass Transfer* 47:1233–1246. doi:10.1016/j.jheatmasstransfer.2003.09.015

- Bašer, T., and J.S. McCartney. 2015. Development of a full-scale soil-borehole thermal energy storage system. In: M. Iskander et al., editors, Proceedings of the International Foundations Conference and Equipment Exposition (IFCEE 2015), San Antonio, TX. 17–21 Mar. 2015. Am. Soc. Civ. Eng., Reston, VA. p. 1608–1617.
- Brandon, T.L., and J.K. Mitchell. 1989. Factors influencing thermal resistivity of sand. *J. Geotech. Eng.* 115:1683–1698. doi:10.1061/(ASCE)0733-9410(1989)115:12(1683)
- Breger, D.B., J.E. Hubbell, H.E. Hasnaoui, and J.E. Sunderland. 1996. Thermal energy storage in the ground: Comparative analysis of heat transfer modeling using U-tubes and boreholes. *Sol. Energy* 56:493–503. doi:10.1016/0038-092X(96)00013-8
- Claesson, J., and G. Hellstrom. 1981. Model studies of duct storage systems. In: J.P. Millhone and E.H. Willis, editors, New energy conservation technologies and their commercialization. Springer-Verlag, Berlin. p. 762–778.
- Dalenbäck, J.-O., and T. Jilar. 1985. Swedish solar seating with seasonal storage: Design, performance and economy. *Int. J. Ambient Energy* 6:123–128. doi:10.1080/01430750.1985.9675454
- Dehkordi, S.E., and R.A. Schincariol. 2014a. Guidelines and the design approach for vertical geothermal heat pump systems: Current status and perspective. *Can. Geotech. J.* 51:647–662. doi:10.1139/cgj-2012-0205
- Dehkordi, S.E., and R.A. Schincariol. 2014b. Effect of thermal-hydrogeological and borehole heat exchanger properties on performance and impact of vertical closed-loop geothermal heat pumpsystems. *Hydrogeol. J.* 22:189–203. doi:10.1007/s10040-013-1060-6
- Dincer, I., and M.A. Rosen. 2007. Energetic, exergetic, environmental and sustainability aspects of thermal energy storage systems. *NATO Sci. Ser.* 234:23–46.
- Diersch, H., D. Bauer, W. Heidemann, W. Rühak, and P. Schätzl. 2011. Finite element modeling of borehole heat exchanger systems. *Comput. Geosci.* 37:1122–1135. doi:10.1016/j.cageo.2010.08.003
- Drake Landing Solar Community. 2015. About DLSC. Drake Landing Solar Community, Okotoks, AB, Canada. <http://www.dlsc.ca/about.htm>.
- Farouki, O.T. 1981. Thermal properties of soils. CRREL Monogr. 81-1. US Army Corps. Eng., Cold Regions Res. Eng. Lab., Hanover, NH.
- Fetter, C.W. 2001. Applied hydrogeology. Prentice Hall, Upper Saddle River, NJ.
- G Tech Earth Sciences Corp. 2004. Geotechnical investigation: Twin Valley Resort. Twin Valley Resort, Ltd., Calgary, AB, Canada.
- Lanini, S., F. Delaleux, X. Py, R. Olivès, and D. Nguyen. 2014. Improvement of borehole thermal energy storage design based on experimental and modelling results. *Energy Build.* 77:393–400. doi:10.1016/j.enbuild.2014.03.056
- Lazarotto, A. 2014. A network-based methodology for the simulation of borehole heat storage systems. *Renew. Energy* 62:265–275. doi:10.1016/j.renene.2013.07.020
- Lee, K.S. 2008. Performance of open borehole thermal energy storage system under cyclic flow regime. *Geosci. J.* 12:169–175. doi:10.1007/s12303-008-0018-5
- Lee, K.S. 2010. A review on concepts, applications, and models of aquifer thermal energy storage systems. *Energies* 3:1320–1334. doi:10.3390/en3061320
- Lee, K.S., and J.J. Sang. 2008. Numerical modeling on the performance of aquifer thermal energy storage system under cyclic flow regime. *Int. J. Green Energy* 5:1–14. doi:10.1080/15435070701845667
- Lu, N. 2001. An analytical assessment on the impact of covers on the onset of air convection in mine wastes. *Int. J. Numer. Anal. Methods Geomech.* 25:347–364.
- Mualem, Y. 1976. A new model predicting the hydraulic conductivity of unsaturated porous media. *Water Resour. Res.* 12:513–522. doi:10.1029/WR012i003p00513
- McCartney, J.S., S. Ge, A. Reed, N. Lu, and K. Smits. 2013. Soil-borehole thermal energy storage systems for district heating. In: Proceedings of the European Geothermal Congress 2013, Pisa, Italy. 3–7 June 2013. [CD-ROM.] Eur. Geothermal Energy Council, Brussels. p. 1–10.
- Molson, J.W., F.O. Frind, and C.D. Palmer. 1992. Thermal energy storage in an unconfined aquifer: 2. Model development, validation, and application. *Water Resour. Res.* 28:2857–2867. doi:10.1029/92WR01472
- Morofsky, E. 2007. History of thermal energy storage. *NATO Sci. Ser.* 234:3–22.
- Newson, J.A., and M.J. O'Sullivan. 2004. Computer modelling of heat and mass flow in steaming ground at Karapiti Thermal Area, New Zealand. In: Proceedings of the 29th Workshop on Geothermal Reservoir Engineering, Stanford, CA. 26–28 Jan. 2004. Stanford Geothermal Program, Stanford, CA.
- Nield, D.A., and A. Bejan. 1992. Convection in porous media. Springer-Verlag, New York.
- Nordell, B., and G. Hellström. 2000. High temperature solar heated seasonal storage system for low temperature heating of buildings. *Sol. Energy* 69:511–523. doi:10.1016/S0038-092X(00)00120-1
- Ohga, H., and K. Mikoda. 2001. Energy performance of borehole thermal energy storage systems. In: R. Lamberts et al., editors, Proceedings of the 7th International IBPSA Conference: Building Simulation, Rio de Janeiro, Brazil. 13–15 Aug. 2001. Int. Building Perform. Simul. Assoc., Brazil.
- O'Sullivan, M.J., K. Pruess, and M.J. Lippmann. 2001. State of the art geothermal reservoir simulation. *Geothermics* 30:395–429. doi:10.1016/S0375-6505(01)00005-0
- Pavlov, G.K., and B.W. Olesen. 2012. Thermal energy storage: A review of concepts and systems for heating and cooling applications in buildings: 1. Seasonal storage in the ground. *HVAC&R Res.* 18:515–538.
- Pruess, K. 1991. TOUGH2: A general-purpose numerical simulator for multiphase fluid and heat flow. LBL-29400. Lawrence Berkeley Lab., Berkeley, CA.
- Sanner, B., and K. Knoblich. 1999. Advantages and problems of high temperature underground thermal energy storage. *Bull. Hydrogeol.* 17:341–348.
- Sanner, B., C. Karytsas, D. Mendrinou, and L. Rybach. 2003. Current status of ground source heat pumps and underground thermal energy storage in Europe. *Geothermics* 32:579–588. doi:10.1016/S0375-6505(03)00060-9
- Schmidt, T., D. Mangold, and H. Muller-Steinhagen. 2003. Seasonal thermal energy storage in Germany. In: Proceedings of ISES Solar World Congress, Göteborg, Sweden. 16–19 June 2003. [CD-ROM.] Int. Solar Energy Soc., Freiberg, Germany.
- Sibbitt, B., T. Onno, D. McClenahan, J. Thornton, J. Brunger, and B. Wong. 2007. The Drake Landing Solar Community project: Early results. In: 2nd Canadian Solar Buildings Conference, Calgary, AB, Canada. 10–14 June 2007. Univ. of Calgary, Calgary, AB.
- Sibbitt, B., D. McClenahan, R. Djebbar, J. Thornton, B. Wong, J. Carriere, and J. Kokko. 2011. Measured and simulated performance of a high solar fraction district heating system with seasonal storage. In: Proceedings of the ISES Solar World Congress, Kassel, Germany. 28 Aug.–2 Sept. 2011. Int. Solar Energy Soc., Freiberg, Germany. p. 1267–1278.
- Sibbitt, B., D. McClenahan, R. Djebbar, J. Thornton, B. Wong, J. Carriere, and J. Kokko. 2012. The performance of a high solar fraction seasonal storage district heating system: Five years of operation. *Energy Procedia* 30:856–865. doi:10.1016/j.egypro.2012.11.097
- Smits, K.M., S.T. Sakaki, S.E. Howington, J.F. Peters, and T.H. Illangasekare. 2013. Temperature dependence of thermal properties of sands across a wide range of temperatures (30–70°C). *Vadose Zone J.* 12(1). doi:10.2136/vzj2012.0033
- Socaciu, L.G. 2011. Seasonal sensible thermal energy storage solutions. *Leonardo Electron. J. Pract. Technol.* 19:49–68.
- Sommer, W., J. Valstar, P. Van Gaans, T. Grotenhuis, and H. Rijnaarts. 2013. The impact of aquifer heterogeneity on the performance of aquifer thermal energy storage. *Water Resour. Res.* 49:8128–8138. doi:10.1002/2013WR013677
- Stauffer, F., P. Bayer, P. Blum, N. Molina-Giraldo, and W. Kinzelbach. 2013. Thermal use of shallow groundwater. CRC Press, Boca Raton, FL.
- Tenma, N., K. Yasukawa, and G. Zvoloski. 2003. Model study of thermal storage system by FEHM code. *Geothermics* 32:603–607. doi:10.1016/S0375-6505(03)00073-7
- van Genuchten, M.Th. 1980. A closed form equation for predicting the hydraulic conductivity of unsaturated soils. *Soil Sci. Soc. Am. J.* 44:892–898. doi:10.2136/sssaj1980.03615995004400050002x
- Wang, X., M. Zheng, W. Zhang, S. Zhang, and T. Yang. 2010. Experimental study of a solar-assisted ground-coupled heat pump system with solar seasonal thermal storage in severe cold areas. *Energy Build.* 42:2104–2110. doi:10.1016/j.enbuild.2010.06.022
- Zhang, R., N. Lu, and Y. Wu. 2012. Efficiency of a community-scale borehole thermal energy storage technique for solar thermal energy. In: R.D. Hryciw et al., editors, Proceedings of the GeoCongress 2012: State of the Art and Practice in Geotechnical Engineering, Oakland, CA. 25–29 Mar. 2012. Am. Soc. Civ. Eng., Reston, VA.